Hainzl, S. (2016): Apparent triggering function of aftershocks resulting from rate-dependent incompleteness of earthquake catalogs. - *Journal of Geophysical Research*, *121*, pp. 6499—6509.

DOI: http://doi.org/10.1002/2016JB013319

AGU PUBLICATIONS

JGR

Journal of Geophysical Research: Solid Earth

RESEARCH ARTICLE
10.1002/2016JB013319

Key Points:
- Derivation of the functional form of aftershock triggering related to incomplete recordings
- The function is found to explain observed aftershock rates very well
- Observed magnitude dependence of the Omori c value likely results only from catalog incompleteness

Supporting Information:
- Supporting Information S1

Correspondence to:
S. Hainzl,
hainzl@gfz-potsdam.de

Citation:
Hainzl, S. (2016), Apparent triggering function of aftershocks resulting from rate-dependent incompleteness of earthquake catalogs, *J. Geophys. Res. Solid Earth*, *121*, 6499–6509, doi:10.1002/2016JB013319.

Received 29 JUN 2016
Accepted 16 AUG 2016
Accepted article online 20 AUG 2016
Published online 5 SEP 2016

Apparent triggering function of aftershocks resulting from rate-dependent incompleteness of earthquake catalogs

Sebastian Hainzl[1]

[1] GFZ German Research Centre for Geosciences, Potsdam, Germany

Abstract The onset of the aftershock decay after main shocks is controversial. Physical models predict that the onset time is stress dependent, and catalog analysis shows a clear increase of the *c* value of the Omori-Utsu law with increasing main shock magnitude. However, earthquake catalogs are known to have variable quality and completeness levels; in particular, they miss events directly after main shocks. Thus, it has been also argued that the delayed onset of recorded aftershock activity triggered by large earthquakes is simply an artifact of the time-varying completeness. Here I utilize a recent approach describing the detection probability of earthquakes as function of the actual earthquake rate. I derive an analytical relation between apparent and true earthquake rate which only depends on the blind time of detection algorithms after the occurrence of an earthquake. This relation is tested and verified for synthetic simulations of Omori-type aftershock sequences. For a comparison, I analyze earthquake sequences occurred in Southern California and Taiwan, finding that the derived analytical decay function consistently explains the empirical aftershock activity in the catalogs. This indicates that the observed scaling of the Omori *c* value is mainly related to catalog incompleteness and not to any underlying physical process.

1. Introduction

Aftershocks are triggered by the coseismic perturbation of stress in the vicinity of a main shock rupture. The rate of triggered aftershocks is found to be approximately constant in the first seconds to hours or even days, followed by a power law decay with time [*Utsu et al.*, 1995]. From physical point of view, a temporal delayed onset can be explained by stress corrosion [*Scholz*, 1968; *Narteau et al.*, 2002] or rate-and-state-dependent frictional nucleation [*Dieterich*, 1994; *Dieterich et al.*, 2000]. Both models predict that a larger amplitude of the perturbation decreases the duration of the initial phase before the onset of the power law decay. The overall empirical aftershock rate $R(t)$ can be usually well described by the Omori-Utsu function, which is a power law with a time-offset parameter c

$$R_0(t) = K\,10^{\alpha(M_m - M_c)}\,(c+t)^{-p}\,, \tag{1}$$

where the exponent p is typically in the range 0.8–1.2 [*Utsu et al.*, 1995]. The productivity depends on the cutoff magnitude M_c of the catalog and increases exponentially with the main shock magnitude M_m. For M_c set to the completeness magnitude of the catalog, the exponent α is found to be typically in the range 0.4–1.1 [*Hainzl and Marsan*, 2008, and references therein]. The *c* value is also found to increase with increasing main shock magnitude. However, it has been shown by sophisticated reprocessing of the recorded seismograms that many additional events can be detected which are missed by routine detection procedures [*Kagan*, 2004; *Kagan and Houston*, 2005; *Peng et al.*, 2006, 2007; *Enescu et al.*, 2007]. This indicates that large *c* values for aftershocks of major earthquakes are at least partially related to incompleteness issues of the operating seismic network. It is less clear whether this similarly affects aftershock sequences triggered by smaller main shocks.

The observed exponential scaling of *c* with the difference between main shock magnitude M_m and M_c, $c \sim 10^{\gamma(M_m - M_c)}$, has been interpreted as a part of the self-similar earthquake generation process [*Shcherbakov et al.*, 2004; *Lippiello et al.*, 2007; *Davidsen et al.*, 2015; *Davidsen and Baiesi*, 2016]. For different main shocks in California, *Shcherbakov et al.* [2004] found that the *c* value scales as function of the lower magnitude cutoff with γ values between 0.75 and 1.05, where γ is determined by a combination of p, the Gutenberg-Richter b value, and an exponent β describing the magnitude dependence of the rate at times $t \gg c$. This range

of values has been also found by *Davidsen et al.* [2015], but the uncertainties of the γ values are large. The observed scaling seems to contradict the expectation of the physical models based on stress corrosion or rate-and-state-dependent frictional nucleation [*Scholz*, 1968; *Dieterich*, 1994; *Narteau et al.*, 2002], where larger stress changes reduce the response time and thus lead to smaller c values and higher rates at short times compared to smaller stress changes. Consequently, larger main shocks are expected to have, if at all, smaller instead of larger c values. However, due to the fact that earthquake-induced stress changes are inhomogeneous in space, the observed aftershock activity is a superposition of stress steps of different sizes which complicates the comparison of the model prediction with the observations [*Helmstetter and Shaw*, 2006; *Marsan*, 2006]. To explain the observed scaling, *Shcherbakov et al.* [2006] suggested a mechanism based on a cascade of stress from large scales to small ones, while *Lippiello et al.* [2007] exploited the dynamical scaling hypothesis originated from a critical dynamics approach, where energy and time depend on each other with self-similar behavior if energy is rescaled by an appropriate power of time. However, independent of the theoretical interpretation, all previous studies show that the empirical aftershock rates are immediately after the main shock approximately the same independently whether $M_m - M_c$ is small or large, which corresponds to $\gamma \approx \alpha/p$ [*Shcherbakov et al.*, 2004; *Lippiello et al.*, 2007; *Davidsen et al.*, 2015; *Davidsen and Baiesi*, 2016].

A common maximum rate of recorded earthquakes can be a direct consequence of rate-dependent incompleteness of earthquake catalogs [*Hainzl*, 2016; *Shelly et al.*, 2016]. *Hainzl* [2016] showed that the maximum rate which can be completely recorded is a function of the blind time Δt after earthquakes, where Δt defines the time period after each earthquake in which the detection algorithm cannot pick smaller-magnitude events. This relation was used by *Hainzl* [2016] to estimate the time-dependent completeness magnitude. In phases of high seismic activity, the general noise level is increased due to earthquake-induced waves (seismic noise) which hamper the detection of individual events. Then the completeness magnitude exceeds the basic detection threshold M_c which is related to the general setup of the monitoring system and the environmental background noise level. Here I use the same approach to determine the time-dependent total rate $R(t)$ of earthquakes above M_c, which can be directly compared to observed aftershock rates. I will show that the resulting decay function is in very good agreement with observations without introducing any c value.

2. Theory

Detection algorithms typically pick seismic waves by comparison of the measured amplitude to the noise level estimated in a longer time window, e.g., in standard phase-picking algorithms based on a short-term average to long-term average ratio [*Earle and Shearer*, 1994]. The overlap of the seismic wave of a preceding larger earthquake with the background window increases the noise level which thus reduces the detectability of subsequent earthquakes. Therefore, the basic assumption of the following derivations is that an earthquake of magnitude M cannot be properly distinguished and thus detected by the seismogram analysis if it occurs less than a blind time Δt after the last event of equal or larger magnitude. This deterministic assumption is used for simplicity. However, I show later in section 3.1 that the derived result similarly works for a probability distribution of the blind time.

For a Poisson process, the probability that no event occurs within Δt is given by $p_d = \exp(-N_{\Delta t})$, where $N_{\Delta t}$ is the expected (average) number of events within time period Δt. Let us assume that the earthquake rate is given by an inhomogeneous Poisson process with functional form $R_0(t)$ for events with magnitude above the general completeness magnitude M_c. The corresponding number of events within period Δt is given by $N_0(t, \Delta t) = \int_{t-\Delta t}^{t} R_0(t)\mathrm{d}t$. Furthermore, the earthquake magnitudes are assumed to be distributed in the range $[M_c, M_{\max}]$ with corresponding complementary cumulative distribution function (ccdf) and probability density function (pdf), respectively. Because ccdf(M) describes the fraction of events with magnitude $\geq M$, the expected number of events with magnitude $\geq M$ in Δt is simply ccdf(M) $N_0(t, \Delta t)$. Thus, the probability to observe an earthquake with magnitude M at time t is

$$p_d(t, M) = e^{-\mathrm{ccdf}(M)\, N_0(t, \Delta t)}. \tag{2}$$

This exponential detection function directly depends on the actual rate and magnitude distribution of the activity. In contrast, the detection function previously introduced by *Ringdal* [1975] and used by *Ogata and Katsura* [2006] and *Omi et al.* [2014] is described by the cumulative of a normal distribution with unrelated empirical parameters (mean and standard deviation).

2.1. Recorded Earthquake Rates

Considering the pdf of earthquake magnitudes, the rate density function for a particular magnitude $M \in [M_c, M_{\max}]$ of the really occurring events becomes $R_0(t, M) = \mathrm{pdf}(M)\, R_0(t)$, while the rate density of recorded magnitude M events is $R(t, M) = R_0(t, M)\, p_d(t, M)$. The total rate of earthquakes recorded in a catalog above M_c is calculated by integrating the latter over the whole magnitude range which results in

$$R(t) = \int_{M_c}^{M_{\max}} R_0(t, M)\, p_d(t, M)\, \mathrm{d}M = \frac{R_0(t)}{N_0(t, \Delta t)} \left(1 - e^{-N_0(t, \Delta t)}\right) \tag{3}$$

see Appendix A for a detailed derivation. For moderate variations of $R_0(t)$ during Δt, $N_0(t, \Delta t)$ can be well approximated by $R_0(t)\Delta t$ and the rate function becomes

$$R(t) \approx \frac{1}{\Delta t} \left(1 - e^{-\Delta t\, R_0(t)}\right) \tag{4}$$

Vice versa, given the observational earthquake rate $R(t)$, the true earthquake rate $R_0(t)$ can be in principle reconstructed by

$$R_0(t) \approx -\ln\left(1 - \Delta t R(t)\right) / \Delta t \tag{5}$$

Note that equations (3)–(5) are valid for arbitrary rate histories.

2.2. Rate-Dependent Apparent Magnitude Distribution

In the same framework, the magnitude distribution of recorded events can be determined for a constant seismicity rate. In particular, the apparent complementary cumulative magnitude distribution function ccdf_a, i.e., the probability for an earthquake with $m \geq M$ in the incomplete catalog, is equal to

$$\mathrm{ccdf}_a(M) = \frac{1 - \exp\left(-R_0\, \Delta t\, \mathrm{ccdf}(M)\right)}{1 - \exp\left(-R_0 \Delta t\right)} \tag{6}$$

(see Appendix B for a detailed derivation). Thus, the resulting distribution depends on the true complementary cumulative distribution function ccdf(M) and the value of $R_0\Delta t$ which is the average number of truly occurring $m \geq M_c$ events in the blind time interval Δt.

For the special case of a Gutenberg-Richter distribution of the magnitudes in the range $[M_c, \infty]$, $\mathrm{ccdf}(M) = 10^{-b(M-M_c)}$, the apparent complementary cumulative magnitude distribution function becomes

$$\mathrm{ccdf}_a(M) = \frac{1 - \exp\left(-R_0\, \Delta t\, 10^{-b(M-M_c)}\right)}{1 - \exp\left(-R_0 \Delta t\right)} \tag{7}$$

depending only on parameter b and $R_0\Delta t$. Figure 1 shows the apparent frequency-magnitude distribution for $b = 1$ and different values of $R_0\Delta t$. For values $R_0\Delta t \leq 0.2$, the apparent distribution is almost indistinguishable from the original one. However, for larger $R_0\Delta t$ values, the distribution significantly deviates from the original one. Small-magnitude events are missed, while the large magnitudes are unaffected. To analyze the effect on b value estimations, I calculate the maximum likelihood value of b for 100 randomly selected events from equation (7) in the case of different $R_0\Delta t$ values [*Aki*, 1965]. The result is shown in the inset of Figure 1. The estimated b value is very close to the true value of 1 in the case of $R_0\Delta t \leq 0.2$ but then starts to become significantly smaller.

This result can be compared with the result of *Hainzl* [2016], who found that the estimated b values start to decrease for rates above approximately 100 $M \geq 2.0$ events per day in Southern California. Here it is found that the deviations occur for $R_0\Delta t \geq 0.2$. Thus, the comparison suggests that the effective blind time is around $\Delta t = 0.002$ days (approximately 170 s) for detections in Southern California.

2.3. Special Case: Omori-Utsu Aftershock Decay

For the special case of an aftershock sequence triggered by a main shock with magnitude M_m at time $t = 0$, the true aftershock rate is assumed to follow the Omori-Utsu function (equation (1)) with $c = 0$. For $t > \Delta t$, the value of $N_0(t, \Delta t)$ is consequently

$$N_0(t, \Delta t) = \begin{cases} K\, 10^{\alpha(M_m - M_c)} \left[t^{1-p} - (t - \Delta t)^{1-p}\right] / (1 - p) & \text{for } p \neq 1, \\ K\, 10^{\alpha(M_m - M_c)} \left[\ln(t) - \ln(t - \Delta t)\right] & \text{for } p = 1. \end{cases} \tag{8}$$

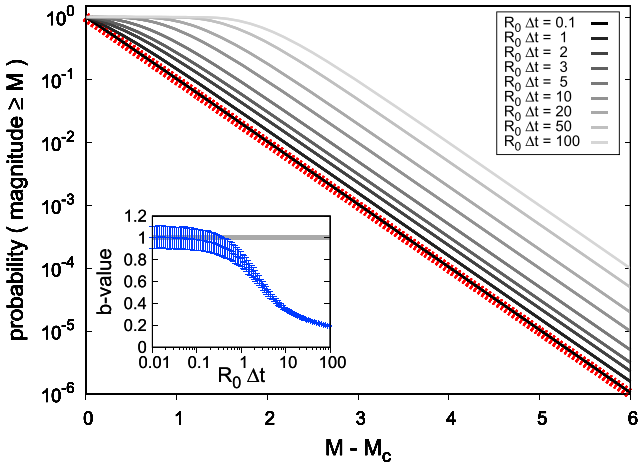

Figure 1. Magnitude distribution for different activity rates (main plot) and corresponding *b* value estimations (inset). The main plot shows the probability for $m \geq M$ events as function of $M - M_c$ (equation (7)), where M_c is the cutoff magnitude. The solid grey curves refer to the apparent distribution inferred from incomplete recordings for different activity rates R_0 of $M \geq M_c$ events (equation (7)), while the dotted red line refers to the true distribution. The inset plot shows the mean ±1 standard deviation of the maximum likelihood estimations of the *b* value for 100 magnitudes randomly selected from the distribution for given $R_0 \Delta t$ value; the horizontal line refers to the true value of $b = 1$.

According to equation (4), the incompletely recorded aftershock rate in the earthquake catalog is for such a power law decay

$$R(t, M_m) = \frac{R_0(t)}{N_0(t, \Delta t)} \left(1 - e^{-N_0(t,\Delta t)}\right) \tag{9}$$

$$\approx \frac{1}{\Delta t} \left[1 - \exp\left(-\Delta t\, K\, 10^{\alpha(M_m - M_c)}\, t^{-p}\right)\right] \tag{10}$$

where equation (8) is used for $N_0(t, \Delta t)$ in equation (9). For equation (10), the integral of $N_0(t, \Delta t)$ is approximated by $R_0(t)\, \Delta t$ independent of the *p* value.

It is important to note that the parameters of the Omori-Utsu function (equation (1)) depend for constant *c* value on the value of M_c if the exponent α of the productivity relation is not equal to the Gutenberg-Richter *b* value [*Shcherbakov et al.*, 2004; *Davidsen et al.*, 2015]. The assumption of self-similarity where aftershock rates only depend on the difference $M_m - M_c$ requires $\alpha = b$. For the main part of our analysis, the value of M_c is fixed and set to the basic detection threshold and thus the assumption of self-similarity is not needed. Only in the analysis of specific aftershock sequences (section 3.2.3), self-similarity is really required. However, for consistency, I assume $\alpha = b$ throughout the remainder of the paper, which is also shown to be in agreement with the observations.

In this case, the parameters are rather well constrained: The *b* (and thus the α value) can be estimated by the *b* value at times of low activity rates [*Hainzl*, 2016]. Furthermore, Δt can be independently estimated from the inverse of the maximum observed earthquake rate, while parameters *K* and *p* are determined by the absolute value and the decay rate at larger times after the main shocks when incompleteness is negligible [*Shcherbakov et al.*, 2004; *Davidsen et al.*, 2015].

3. Application

3.1. Test for Synthetic Sequences

The analytical results are tested by synthetic simulations of aftershock sequences according to the Omori-Utsu law and the epidemic-type aftershock sequence (ETAS) model [*Ogata*, 1988]. For this, I assume a Gutenberg-Richter distribution in the range $[M_c, M_c + 5.5]$ with $b = 1$ and set $K = 0.002$, $\alpha = b$, $p = 1.0$, and $c = 0.01$ s. To simulate the detection problem in phases of overlapping seismograms, I apply two alternative procedures:

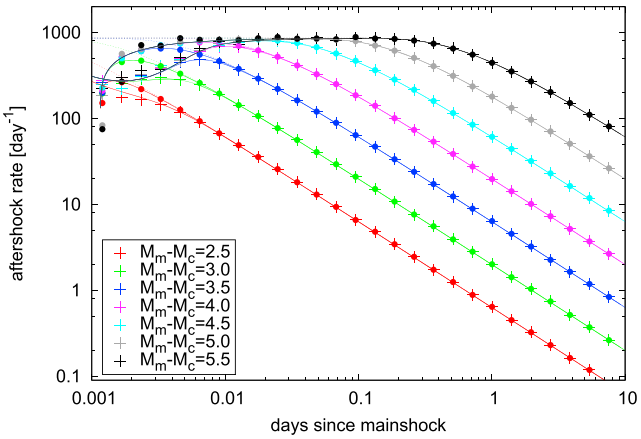

Figure 2. Result of synthetic aftershock sequences simulated by a pure power law decay (equation (1) with $c=0$, $K=0.002$, $\alpha=1$, and $p=1$), where events are removed by procedure P1 (points) or P2 (crosses) with $\Delta t=100$ s. The values represent the average result for $10^{7.5-(M_m-M_c)}$ simulations for each main shock magnitude value M_m. For comparison, the lines show the theoretical functions (solid = equation (9); dotted = equation (10)) corresponding to the same parameters. Note that the theoretical result of equation (9) only leads to different solutions for procedures P1 and P2 at times shorter than 0.01 day.

(P1) An event is removed if another event with larger or equal magnitude occurred within the preceding time period Δt; in particular, a magnitude M_i event occurred at time t_i is deleted, if another event with magnitude $M_j \geq M_i$ occurred with time $t_j \in [t_i - \Delta t, t_i]$. This choice is equivalent to a fixed Δt value and a probability to be undetected of $p_{ud}(t_i - t_j, \Delta t) = H(\Delta t - (t_i - t_j))$, with H being the Heaviside function.

(P2) As an alternative, I assume that the probability to be undetected p_{ud} is not binary but a smooth function of the time difference $t_i - t_j$ to preceding larger earthquakes. Here I assume for simplicity an exponential detection function $p_{\mathrm{ud}}(t_i - t_j, \Delta t) = \exp(-[t_i - t_j]/\Delta t)$. This is equivalent to the assumption of an exponential probability distribution of the blind time with a mean value of Δt. Accounting for all preceding events with magnitude $M_j \geq M_i$, event i is randomly chosen to be removed according to the probability $p_{\mathrm{ud}}(t_i - t_j, \Delta t)$.

In both cases, I choose $\Delta t=100$ s as exemplary value and analyze the remaining (recorded) aftershocks for main shock magnitudes M_m varying between $M_c + 2.5$ and $M_c + 5.5$. In each case, I run 1000 Monte Carlo simulations, where earthquake magnitudes and occurrence times are randomly selected from their probability distributions. The resulting earthquake rates of the different simulations are averaged in time bins. The result is shown in Figure 2 for the simulations of the Omori-Utsu decay, where the simulations (symbols) are compared with equation (9) (solid lines) and its approximation (equation (10), dotted lines). It is important to note that with $N_0(t, \Delta t) = \int_0^\infty R_0(t - \tau) p_{\mathrm{ud}}(\tau) \mathrm{d}\tau$, equation (9) perfectly matches the results of the incomplete catalogs independent of the procedure P1 or P2 for removing the events. Although the analytical derivation is done above only for P1, equation (9) is also valid for more realistic smooth detection functions, respectively probability distributions of Δt. Also, the approximation (equation (10)) works well in both cases for times larger than 0.01 day but leads to an overestimation at smaller times. At small times the approximation does not work because the rate $R_0(t)$ starts to strongly decay over time period Δt and thus $R_0(t)\Delta t$ underestimates $N_0(t, \Delta t)$ significantly and the recorded rates fall below $1/\Delta t$. However, independent of the main shock magnitude, the absolute rate is limited by $1/\Delta t$ and main shocks of different size mainly differ in the duration of the initial phase with almost constant rate.

The corresponding analysis of the ETAS simulations leads to similar results. This is shown in Figure S1 of the supporting information for ETAS simulations with parameters as above which are started with a main shock of magnitude M_m. For infinite long aftershock triggering, $p = 1$ would lead to an instability with accelerated rates at long times, but for finite triggering times, the chosen ETAS parameters lead to stable conditions. In particular, the branching parameter (average number of triggered events) is 0.3 and 0.5 for a triggering time of 1 and 10^6 years, respectively. The additional secondary aftershock triggering leads to an increased number of simulated aftershocks. However, after removing undetectable events according to procedure P1/P2 with $\Delta t = 100$ s, the maximum recorded rate is the same as for the simple Omori-Utsu decay, namely, $1/\Delta t$.

The overall activity is fit with slightly different α and p values than the input values for the direct aftershocks, namely, $\alpha = 1.05$ and $p = 0.95$ (input: $\alpha = p = 1$). In contrast, the recorded direct aftershocks of the main shocks are well fitted by the input ETAS parameters, but the maximum rate of direct aftershocks is less than the maximum rate of the total activity and only the latter is related to the true Δt value. Fitting equation (9)/(10) to the direct aftershocks leads consequently to a larger apparent value of Δt, namely, 180 s instead of 100 s.

3.2. Application to Observations

To test the derived apparent triggering function equation (9)/(10) for empirical catalog data, I use aftershock sequences selected from high-quality data sets from California and Taiwan and analyze them similarly to the synthetic data.

3.2.1. Data and Cluster Selection

I analyze earthquake clusters recorded in Southern California and Taiwan. Particularly, I use the updated relocated Southern California catalog containing earthquakes from 1981 to 2014 [*Hauksson et al.*, 2012] with a cutoff magnitude of $M_c = 2.0$. The data consist of 118,495 earthquakes above this magnitude threshold. As an independent data set, I also analyze the catalog published by *Wu et al.* [2008] which consists of relocated earthquakes in Taiwan between 1991 and 2005. Using the same cutoff magnitude of $M_c = 2.0$ for shallow events with depth less than 50 km, this data set consists of 151,393 events.

For the aftershock selection, I use a recently established scheme based on nearest-neighbor distances [*Baiesi and Paczuski*, 2004, 2005; *Zaliapin et al.*, 2008; *Zaliapin and Ben-Zion*, 2013]. The method quantifies the correlation between an event i and a following event j by its magnitude-weighted space-time distance $n_{ij} = (t_j - t_i)\,|\vec{x}_j - \vec{x}_i|^d\,10^{-bM_i}$ with $t, \vec{x}, M$ being the time, location, and magnitude of the events. Here I use epicenter distances with a fractal dimension of $d = 1.6$ and b values resulting from maximum likelihood estimations. Among all events i preceding j, the identification of the (most likely) trigger of j results from selecting that event with the lowest n_{ij} value. To distinguish between triggered and background activity, a threshold value of $\log(n_c) = 7.0$ is found to be appropriate [*Moradpour et al.*, 2014]; i.e., only events with $n_{ij} \le n_c$ are considered as plausible main shock-aftershock pairs. By means of ETAS simulations, this aftershock detection method used here has been previously demonstrated to be robust with respect to (1) changes of the involved parameters of the method, (2) catalog incompleteness, and (3) location errors [*Zaliapin and Ben-Zion*, 2013]. The method has also the advantage that it can identify the directly triggered aftershocks and not only the overall aftershock activity. For a better comparison with the theoretical curves for simple Omori-type aftershock decays (equation (9)/(10)), I will show in the following only the results for directly triggered aftershocks. However, similar results are found for the overall aftershock activity as well as for aftershocks selected by an alternative, window-based cluster selection method as shown in the supporting information.

3.2.2. Dependence of the Aftershock Activity on M_m

For fixed M_c=2.0, I show in this section that the observed activity is in good agreement with the theoretical predictions for the apparent frequency-magnitude distribution and aftershock decay function. For the analysis of the frequency-magnitude distribution, I first estimate the local rate at the occurrence time of each earthquake in the catalog. This is done by the determination of the time interval of the 10 closest events in time [see *Hainzl*, 2016]. It results in the paired information of magnitude and local rate for each event $(M_i, \hat{R}_i)$. The event magnitude M_i is sorted to the corresponding logarithmic rate bin that includes $\hat{R}_i$. For all data sets analyzed in this study, Figure 3a shows the maximum likelihood estimates of the b value in dependence on the local rate. In all cases, the b value estimate is rather stable at low rates and starts to decrease for rates larger than approximately 100 events per day. This decrease is attributed to more and more incomplete detections for increasing seismicity levels [*Hainzl*, 2016]. The estimates for low rates, which are assumed to represent the true b value, differ significantly for the different data sets: $b = 0.8$ for Taiwan, $b = 1.0$ for Southern California, and $b = 1.3$ for the two specific aftershock sequences of the M7.3 Landers and the M7.1 Hector Mine main shocks which are analyzed in section 3.2.3. Figure 3b shows the complementary cumulative frequency-magnitude distribution for three wider rate bins in the case of the Southern California data set. For the lowest rate bin, the distribution can be well fitted by the Gutenberg-Richter distribution with b=1.0. However, for the two larger rate bins, significant deviations for small magnitudes are observed. The observed shape of the distribution for the rate range between 200 and 700 events per day can be well fitted by the theoretical distribution (equation (7)) with $R_0\,\Delta t = 1.0$, while $R_0\,\Delta t = 3.0$ well approximates the observed one for rates above 700 events per day.

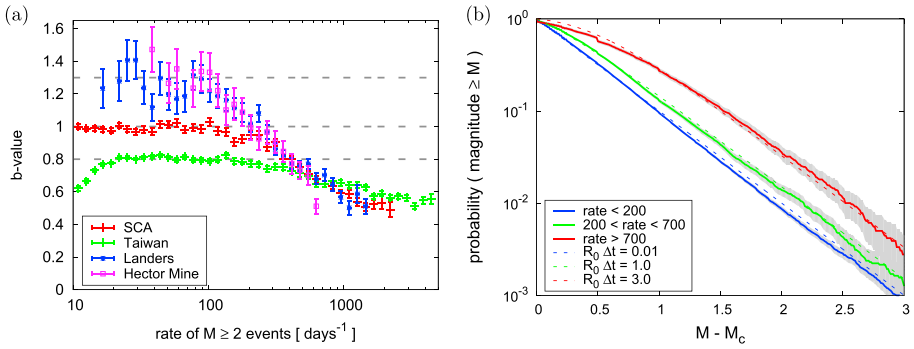

Figure 3. (a) Estimated b value for the analyzed data sets as a function of the local earthquake rate. The horizontal dashed lines refer to b values of 0.8, 1.0, and 1.3, and the error bars refer to ±1 standard deviation. (b) Frequency-magnitude distribution for three ranges of the local activity rate (events per day) in Southern California (solid lines, $M_c = 2.0$). The gray shaded regions refer to the 95% confidence interval. For comparison, the theoretical distribution (equation (7)) is shown by dashed lines for the three levels $R_0\Delta t = 0.01$, 1.0, and 3 with $b = 1.0$.

Figure 4 shows the result for the stacked and averaged aftershock rate following main shocks of different sizes in Southern California and Taiwan. In both cases, the result looks quite similar. In the double logarithmic plot, the aftershock rates are, at larger times, almost equidistantly separated according to the main shock magnitude, which indicates an exponential increase of the productivity with main shock magnitude. However, at short times, all curves start to collapse and the recorded activity has very similar levels independent whether the main shock magnitude is above 7 or below 4.5. Furthermore, all rates are found to be bounded at approximately $r_{max} = 500$ and 700 events per day in Southern California and Taiwan, respectively. The higher value in Taiwan coincides with shorter delay times of the power law onset. Another characteristic is the apparent low rate of the very first aftershock which falls below the observed maximum rate at intermediate times.

All these characteristics can be well explained by the triggering function related to rate-dependent incompleteness (equation (9)/(10)). Here α is again set to the b value to account for self-similarity, with b value defined by the estimated value at low activity levels, i.e., $\alpha = 1.0$ and 0.8 for Southern California and Taiwan, respectively (see Figure 3a). The other parameters are constrained either by the maximum observed rate of $M \geq 2$ earthquakes (Δt) or the absolute values and rate changes of the aftershock activity at later times when the estimates are not significantly affected by incompleteness (K, p). The fits to the observed data yield the parameters $K = 0.003$, $\alpha = b = 1.0$, $\Delta t = 170$ s, and $p = 0.95$ for Southern California and $K = 0.003$, $\alpha = b = 0.8$, $\Delta t = 130$ s, and $p = 1.05$ for Taiwan. The corresponding decay functions of equation (9)/(10) are shown by lines in Figure 4 for the average main shock magnitude in each magnitude bin. Despite the different b values (α values), the fits are very good in both cases, which indicates that the assumption of self-similarity seems to be consistent with the data. Furthermore, the value of $\Delta t = 170$ s for California is in good agreement with the expectation from the b value analysis (see section 2.2).

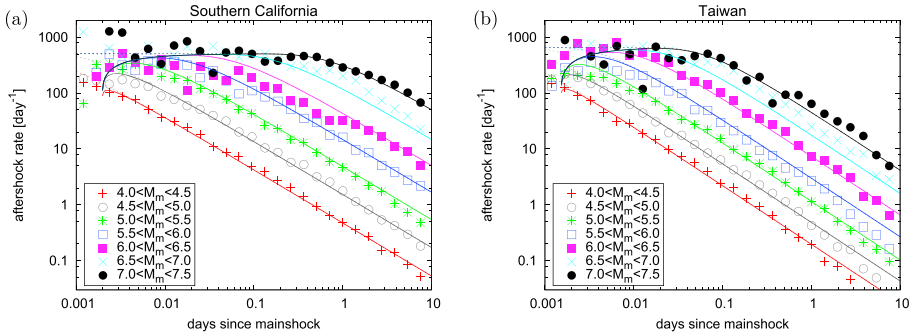

Figure 4. Average rates of direct $M \geq 2.0$ aftershocks in (a) Southern California and (b) Taiwan sorted for different main shock magnitudes M_m. For comparison, the lines show the theoretical functions for the average main shock magnitude in each bin (solid = equation (9); dashed = equation (10)), with parameters $K = 0.003$, $\alpha = b = 1.0$, $\Delta t = 170$ s, and $p = 0.95$ (Figure 4a) and $K = 0.003$, $\alpha = b = 0.8$, $\Delta t = 130$ s, and $p = 1.05$ (Figure 4b).

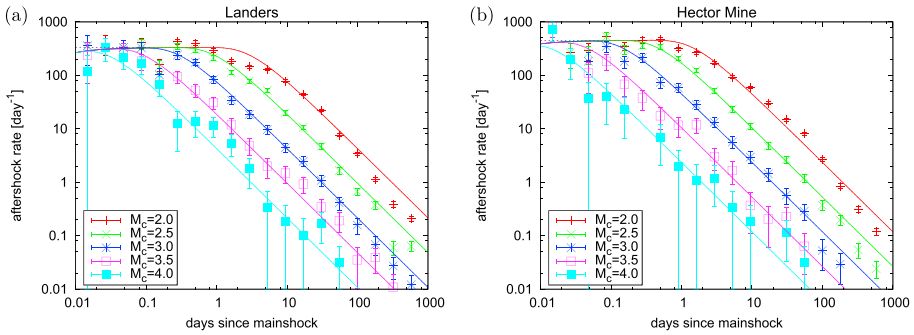

Figure 5. Average rates of direct aftershock of the (a) Landers and (b) Hector Mine aftershock sequences sorted for different cutoff magnitudes. For comparison, the lines show the theoretical functions (solid = equation (9); dashed = equation (10)) with parameter values $K = 0.0002$, $\alpha = b = 1.3$, $p = 1.3$, and $\Delta t = 260$ s (Figure 5a) and $\Delta t = 190$s (Figure 5b).

The analyses of the overall aftershock activity (including aftershocks of aftershocks) yield very similar results. The same is found if an alternative aftershock selection procedure is used which is based on a window approach. The results for these cases are shown in the supporting information (Figures S2–S5). Although estimated parameter values depend on the particular choice of the data selection, all general results concerning the shape of the decay and the data fit remain the same.

3.2.3. Single Aftershock Sequences With Variable M_c

Due to self-similarity ($\alpha = b$), the triggering function for recorded aftershocks (equation (9)/(10)) depends only on the difference between the main shock and cutoff magnitude, $M_m - M_c$, because both $N_0(t, \Delta t)$ and $R_0(t)$ depend only on $M_m - M_c$ (see equations (1) and (8)). Thus, the function should hold not only for different main shock magnitudes with fixed M_c value as shown above but also for the same main shock with different M_c values. To demonstrate this, I select as examples the specific aftershock sequences of the two well-known 1992 M7.3 Landers and the 1999 M7.1 Hector Mine events in Southern California. For each of these examples, I choose M_c values varying between 2.0 and 4.0 and calculate the rate of $M \geq M_c$ aftershocks in consecutive time bins. Figure 5 shows the corresponding results. Because the number of involved aftershocks is significantly reduced in comparison to the stacked data analyzed above, wider time bins are used in a larger time period up to 1000 days. Nevertheless, the results show that the triggering function of equation (9)/(10) is found to explain these data equally well.

4. Discussion

Despite the success in reproducing the main characteristics of recorded seismicity in phases of high activity, the applied approach is certainly a strong simplification of the complex problem of earthquake detections. Thus, it cannot be expected that it can reproduce all details. In particular, the detection quality is often changing with time due to manual interference and new detection algorithms. The modeling of these changes requires detailed information which might be often not available.

A questionable simplification of the approach is that the blind time Δt after events is likely not a constant but increases with the earthquake magnitude. While an analytical consideration of this case is difficult, I tested this issue for synthetic simulations, where I extended a basic Δt value by estimates of the rupture duration of earthquakes in the range between magnitude 2.0 and 7.5. I found no significant effect on the results.

Another simplification of the approach is that preceding earthquakes are not assumed to disturb the detection of subsequent larger-magnitude events. However, the occurrence of smaller events within Δt will also increase the noise level and can lead to a missed detection because the signal-to-noise ratio (SNR) falls below the required threshold (SNR_{min}). Thus, more realistically, ccdf(M) in the detection function (equation (2)) has to be replaced by ccdf($M - \Delta M$) with $M - \Delta M$ defining the magnitude of an event which on average leads to $SNR = SNR_{min}$ for a subsequent magnitude M event occurring within Δt. For a Gutenberg-Richter distribution, it can be easily shown that this leads to equation (10) where Δt is replaced by $10^{b\,\Delta M}\,\Delta t_{true}$. Thus, the estimates of Δt in this paper would be related to a true value of $\Delta t_{true} = 10^{-b\,\Delta M}\,\Delta t$. Consequently, the true blind time might be only in the order of 10–30 s for $\Delta t = 100$ s and $\Delta M = 0.5$–1.0.

5. Conclusions

Although it is well known that empirical earthquake catalogs lack early aftershocks [*Kagan*, 2004; *Kagan and Houston*, 2005; *Peng et al.*, 2006, 2007; *Enescu et al.*, 2007; *Hainzl*, 2016], it is controversial whether this is the only reason for the observed magnitude dependence of the c value of the Omori-Utsu decay function (equation (1)) [*Shcherbakov et al.*, 2004; *Lippiello et al.*, 2007; *Davidsen et al.*, 2015; *Davidsen and Baiesi*, 2016]. In principle, the c value can provide important clues about the stress state and the underlying earthquake generation process [*Scholz*, 1968; *Dieterich*, 1994; *Narteau et al.*, 2002; *Shcherbakov et al.*, 2006; *Lippiello et al.*, 2007; *Narteau et al.*, 2008, 2009]. However, the time-varying completeness of empirical earthquake catalogs can bias the results and thus has to be considered in detail. A quantitative analysis of its effects has been so far hampered by the fact that incompleteness was only empirically quantified by deviations from the Gutenberg-Richter distribution at early times [*Kagan*, 2004; *Helmstetter et al.*, 2006; *Agnew*, 2015]. In this study, I show that based on the simple theory of rate-dependent incompleteness [*Hainzl*, 2016], theoretical relations between the true and the apparent frequency-magnitude distribution and rate function of detected events in a catalog can be established. It only depends on the effective blind time Δt of the detection algorithm utilized by the seismic monitoring network. Applied to a power law decay of aftershocks (Omori-Utsu decay with $c=0$), the theoretical triggering function of detected aftershocks predicts a maximum recorded aftershock rate independent of the main shock magnitude. Based on synthetic aftershock simulations, it is found that this theoretical function holds not only in the case of a fixed blind time Δt but also for more realistic distributions of blind times with a mean value of Δt.

The theoretical triggering function allows a direct comparison with the detected aftershocks in empirical earthquake catalogs. The results show that it very well fits all the main characteristics of the empirical data, namely, a temporally increasing rate for early aftershocks, a common maximum rate independent of the main shock magnitude, and the apparent scaling of the onset time of the power law decay with main shock magnitude. These characteristics can be all explained without any additional free parameter, just with parameter Δt replacing the c parameter. The estimated values of Δt range between 90 and 170 s for Southern California and 60–130 s for Taiwan depending on the data selection procedure. This estimation is in agreement with $r_{\max}$ estimates for complete records based on the b value analysis in Southern California [*Hainzl*, 2016]. This consistency and the success to explain the empirical data without introducing an additional scaling parameter γ indicates that the empirically observed c value scaling with main shock magnitude, $c \sim 10^{\gamma} M_m$, is likely related to catalog incompleteness and does not represent the underlying earthquake generation process. The derived theoretical relation between the true and recorded rates (equation (3)) and the specific triggering function for power law decays of aftershock activity (equation (9)/(10)) offers an opportunity to avoid erroneous parameter estimations and conclusions based on the analysis of empirical catalog data.

Appendix A: Derivation of the Incomplete Rate Function

Let us assume that the true earthquake rate is $R_0(t)$ and the earthquakes are distributed in the range $[M_c, M_{\max}]$ with the corresponding complementary cumulative distribution function, ccdf(M), and the probability density function pdf(M). General properties of these distribution functions are that ccdf(M_c) = 1, ccdf($M_{\max}$) = 0, and that pdf(M) = $-\frac{\mathrm{d}}{\mathrm{d}M}$ccdf($M$). With detection probability p_d defined in equation (2), the rate of earthquakes recorded in a catalog thus becomes

$$\begin{aligned} R(t) &= \int_{M_c}^{M_{\max}} R_0(t,M)\, p_d(t,M)\, \mathrm{d}M \\ &= R_0(t) \int_{M_c}^{M_{\max}} \mathrm{pdf}(M)\, e^{-\mathrm{ccdf}(M) N_0(t,\Delta t)}\, \mathrm{d}M \\ &= \frac{R_0(t)}{N_0(t,\Delta t)} \int_{M_c}^{M_{\max}} \frac{\mathrm{d}}{\mathrm{d}M} e^{-\mathrm{ccdf}(M) N_0(t,\Delta t)}\, \mathrm{d}M \\ &= \frac{R_0(t)}{N_0(t,\Delta t)} \left(e^{-\mathrm{ccdf}(M_{\max}) N_0(t,\Delta t)} - e^{-\mathrm{ccdf}(M_c) N_0(t,\Delta t)} \right) \\ &= \frac{R_0(t)}{N_0(t,\Delta t)} \left(1 - e^{-N_0(t,\Delta t)} \right) \end{aligned} \tag{A1}$$

Appendix B: Derivation of the Rate-Dependent Apparent Magnitude Distribution

Let us assume that the true constant earthquake rate is R_0 and that the earthquakes are distributed in the range $[M_c, M_{\max}]$ with the corresponding complementary cumulative distribution function, ccdf(M), and the probability density function pdf(M) (see Appendix A for their general properties). The apparent complementary cumulative distribution ccdf_a function of the earthquake magnitudes in the recorded catalog can be calculated by

$$\begin{aligned}\mathrm{ccdf}_a(M) &= \tilde{C}\int_M^{M_{\max}} \mathrm{pdf}(m)\, p_d(m)\, \mathrm{d}m \\ &= \tilde{C}\int_M^{M_{\max}} \mathrm{pdf}(m)\, e^{-\mathrm{ccdf}(m)R_0\Delta t}\, \mathrm{d}m \\ &= \tilde{C}\frac{1}{R_0\Delta t}\left(e^{-\mathrm{ccdf}(M_{\max})R_0\Delta t} - e^{-\mathrm{ccdf}(M)R_0\Delta t}\right) \\ &= C\left(1 - e^{-R_0\,\Delta t\mathrm{ccdf}(M)}\right)\end{aligned} \tag{B1}$$

with $\tilde{C}$, C normalization constants ($C = [1 - \exp(-R_0\Delta t)]^{-1}$).

Acknowledgments
The catalog of Southern California had been downloaded from the Southern California Earthquake Data Center (SCEDC, http://scedc.caltech.edu/research-tools/alt-2011-dd-hauksson-yang-shearer.html) accessed on 15 March 2016. The data from Taiwan are published by *Wu et al.* [2008]. I am grateful to two anonymous reviewers and Jörn Davidsen for their valuable comments.

References

Agnew, D. C. (2015), Equalized plot scales for exploring seismicity data, *Seismol. Res. Lett.*, *86*, 1412–1423.
Aki, K. (1965), Maximum likelihood estimate of b in the formula $\log N = a - bM$ and its confidence limits, *Bull. Earthquake Res. Inst.*, *43*, 237–239.
Baiesi, M., and M. Paczuski (2004), Scale-free networks of earthquakes and aftershocks, *Phys. Rev. E*, *69*, 066106, doi:10.1103/PhysRevE.69.066106.
Baiesi, M., and M. Paczuski (2005), Complex networks of earthquakes and aftershocks, *Nonlin. Process. Geophys.*, *12*, 1–11.
Davidsen, J., C. Gu, and M. Baiesi (2015), Generalized Omori-Utsu law for aftershock sequences in Southern California, *Geophys. J. Int.*, *201*, 965–978.
Davidsen, J., and M. Baiesi (2016), Self-similar aftershock rates, *Phys. Rev. E*, *94*(2), 022314, doi:10.1103/PhysRevE.94.022314.
Dieterich, J. H. (1994), A constitutive law for rate of earthquake production and its application to earthquake clustering, *J. Geophys. Res.*, *99*, 2,601–2,618.
Dieterich, J. H., V. Cayol, and P. Okubo (2000), The use of earthquake rate changes as a stress meter at Kilauea volcano, *Nature*, *408*, 457–460.
Earle, P. S., and P. M. Shearer (1994), Characterization of global seismograms using an automatic-picking algorithm, *Bull. Seismol. Soc. Am.*, *84*(2), 366–376.
Enescu, B., J. Mori, and M. Miyazawa (2007), Quantifying early aftershock activity of the 2004 mid-Niigata Prefecture earthquake (M_w6.6), *J. Geophys. Res.*, *112*, B04310, doi:10.1029/2006JB004629.
Hainzl, S. (2016), Rate-dependent incompleteness of earthquake catalogs, *Seismol. Res. Lett.*, *87*, 337–344.
Hainzl, S., and D. Marsan (2008), Dependence of the Omori-Utsu law parameters on main shock magnitude: Observations and modeling, *J. Geophys. Res.*, *113*, B10309, doi:10.1029/2007JB005492.
Hauksson, E., W. Yang, and P. Shearer (2012), Waveform relocated earthquake catalog for southern California (1981 to 2011), *Bull. Seismol. Soc. Am.*, *102*, 2239–2244, doi:10.1785/0120120010.
Helmstetter, A., and B. E. Shaw (2006), Relation between stress heterogeneity and aftershock rate in the rate-and-state model, *J. Geophys. Res.*, *111*, B07304, doi:10.1029/2005JB004077.
Helmstetter, A., Y. Y. Kagan, and D. D. Jackson (2006), Comparison of short-term and time-independent earthquake forecast models for southern California, *Bull. Seismol. Soc. Am.*, *96*(1), 90–106.
Kagan, Y. Y. (2004), Short-term properties of earthquake catalogs and models of earthquake source, *Bull. Seismol. Soc. Am.*, *94*(4), 1207–1228.
Kagan, Y. Y., and H. Houston (2005), Relation between mainshock rupture process and Omori's law for aftershock moment release rate, *Geophys. J. Int.*, *163*(3), 1039–1048.
Marsan, D. (2006), Can coseismic stress variability suppress seismicity shadows? Insights from a rate-and-state friction model, *J. Geophys. Res.*, *111*, B06305, doi:10.1029/2005JB004060.
Moradpour, J., S. Hainzl, and J. Davidsen (2014), Nontrivial decay of aftershock density with distance in Southern California, *J. Geophys. Res.*, *119*, 5518–5535, doi:10.1002/2014JB010940.
Narteau, C., P. Shebalin, and M. Holschneider (2002), Temporal limits of the power law aftershock decay rate, *J. Geophys. Res.*, *107*, B2359, doi:10.1029/2002JB001868.
Narteau, C., P. Shebalin, and M. Holschneider (2008), Loading rates in California inferred from aftershocks, *Nonlin. Process. Geophys.*, *15*, 245–263.
Narteau, C., S. Byrdina, P. Shebalin, and D. Schorlemmer (2009), Common dependence on stress for the two fundamental laws of statistical seismology, *Nature*, *462*, 642–646.
Lippiello, E., M. Bottiglieri, C. Godano, and L. de Arcangelis (2007), Dynamical scaling and generalized Omori law, *Geophys. Res. Lett.*, *34*, L23301, doi:10.1029/2007GL030963.
Ogata, Y. (1988), Statistical models for earthquake occurrence and residual analysis for point processes, *J. Am. Stat. Assoc.*, *83*, 9–27.
Ogata, Y., and K. Katsura (2006), Immediate and updated forecasting of aftershock hazard, *Geophys. Res. Lett.*, *33*, L10305, doi:10.1029/2006GL025888.
Omi, T., Y. Ogata, Y. Hirata, and K. Aihara (2014), Estimating the ETAS model from an early aftershock sequence, *Geophys. Res. Lett.*, *41*, 850–857, doi:10.1002/2013GL058958.

Peng, Z. G., J. E. Vidale, and H. Houston (2006), Anomalous early aftershock decay rate of the 2004 Mw6.0 Parkfield, California, earthquake, *Geophys. Res. Lett.*, *33*(17), L17307, doi:10.1029/2006GL026744.

Peng, Z. G., J. E. Vidale, M. Ishii, and A. Helmstetter (2007), Seismicity rate immediately before and after main shock rupture from high-frequency waveforms in Japan, *J. Geophys. Res.*, *112*(B3), B03306, doi:10.1029/2006JB004386.

Press, W. H., S. A. Teukolsky, W. T. Vetterling, and B. P. Flannery (1992), *Numerical Recipes in C: The Art of Scientific Computing*, 2nd ed., Cambridge Univ. Press, New York.

Ringdal, F. (1975), On the estimation of the seismic detection threshold, *Bull. Seismol. Soc. Am.*, *65*, 1631–1642.

Scholz, C. H. (1968), Microfractures, aftershocks, and seismicity, *Bull. Seismol. Soc. Am.*, *58*, 1117–1130.

Shcherbakov, R., D. L. Turcotte, and J. B. Rundle (2004), A generalized Omori's law for earthquake aftershock decay, *Geophys. Res. Lett.*, *31*, L11613, doi:10.1029/2004GL019808.

Shcherbakov, R., D. L. Turcotte, and J. B. Rundle (2006), Scaling properties of the Parkfield aftershock sequence, *Bull. Seismol. Soc. Am.*, *96*, S376–S384.

Shelly, D. R., W. Ellsworth, and D. P. Hill (2016), Fluid faulting evolution in high definition: Connecting fault structure and frequency-magnitude variations during the 2014 Long Valley Caldera, California, earthquake swarm, *J. Geophys. Res.*, *121*, 1776–1795.

Utsu, T., Y. Ogata, and R. S. Matsu'ura (1995), The centenary of the Omori formula for a decay of aftershock activity, *J. Phys. Earth*, *43*, 1–33.

Wells, D. L., and K. J. Coppersmith (1994), New empirical relationships among magnitude, rupture length, rupture width, rupture area, and surface displacement, *Bull. Seism. Soc. Am.*, *84*, 974–1002.

Wu, Y.-M., C.-H. Chang, L. Zhao, T.-L. Teng, and M. Nakamura (2008), A comprehensive relocation of earthquakes in Taiwan from 1991 to 2005, *Bull. Seismol. Soc. Am.*, *98*, 1471–1481, doi:10.1785/0120070166.

Zaliapin, I., and Y. Ben-Zion (2013), Earthquake clusters in southern California—I: Identification and stability, *J. Geophys. Res.*, *118*, 2847–2864.

Zaliapin, I., A. Gabrielov, V. Keilis-Borok, and H. Wong (2008), Clustering analysis of seismicity and aftershock identification, *Phys. Rev. Lett.*, *101*, 018501, doi:10.1103/PhysRevLett.101.018501.